



# CryoClim Snow Products Documentation

CryoClim snow sub-service by MET Norway and NR



15 January 2004

Note

Note no.

**BAMJO/05/23**

Authors

**Rune Solberg, Øystein Rudjord, Arnt-Børre Salberg, Jarle Hamar Reksten, Mari Anne Killie, Steinar Eastwood, Atle Sørensen, Carlo Marin, Valentina Premier**

Date

**10 January 2023**



### **Norsk Regnesentral**

Norsk Regnesentral (Norwegian Computing Center, NR) is a private, independent, non-profit foundation established in 1952. NR carries out contract research and development projects in information and communication technology and applied statistical-mathematical modelling. The clients include a broad range of industrial, commercial and public service organisations in the national as well as the international market. Our scientific and technical capabilities are further developed in co-operation with The Research Council of Norway and key customers. The results of our projects may take the form of reports, software, prototypes, and short courses.

### **Meteorologisk institutt**

Meteorologisk institutt (Norwegian Meteorological Institute, MET Norway) is the meteorological service for both The Military and the Civil Services in Norway, as well as the public. Our mission is to protect life, property and the environment, and to provide the meteorological services required by society. Our vision is that the institute is to be a centre of excellence on meteorological conditions relevant for Norway, and the results of its competence are to be used as a tool to the general public, the authorities, commerce and industry in their decision-making process on a short-term basis and for the future.

### **Eurac Research**

Eurac Research (Bolzano, Italy) addresses the greatest challenges of the future: keeping societies healthy, fostering intact environments, promoting sustainable energy and developing well-functioning political and social systems. Seeking answers through interaction between a variety of disciplines, we develop concrete solutions for regional problems which can then be applied globally. We continually strive to open new paths with science and innovation, by responding to society's complex questions with answers geared to the needs of people.

**Norsk Regnesentral**  
Norwegian Computing Center  
Postboks 114, Blindern  
NO-0314 Oslo, Norway

**Besøksadresse**  
*office address*  
Gaustadalleen 23a  
NO-0373 Oslo, Norway

**Telefon** · telephone  
(+47) 22 85 25 00  
**Telefaks** · telefax  
(+47) 22 69 76 60

**Bankkonto** · bank account  
8200.01.48888  
**Org.nr.** · enterprise no.  
NO 952125001 VAT

**Internett** · internet  
[www.nr.no](http://www.nr.no)  
**E-post** · e-mail  
[nr@nr.no](mailto:nr@nr.no)

<b>Title</b>	<b>CryoClim Snow Products Documentation</b>
<b>Authors</b>	<b>Rune Solberg, Øystein Rudjord, Arnt-Børre Salberg, Jarle Hamar Reksten, Mari Anne Killie, Steinar Eastwood, Atle Sørensen, Carlo Marin, Valentina Premier</b>
Quality assurance	Internal
Date	10 January 2023
Year	2023
Publication number	BAMJO/05/23

### **Abstract**

The CryoClim project (2008-2013) developed an operational service for long-term systematic climate monitoring of the cryosphere, including a sub-service for snow. This sub-service is based on algorithms for single-sensor retrieval of snow cover extent from optical and passive microwave radiometer (PMR) data, and the fusion of those with a novel multi-sensor multi-temporal algorithm. The product was advanced in the Sentinel4CryoClim project (phase 1 and 2; 2015-2018) mitigating a number of initial weaknesses and adding uncertainty information. The original product was binary. The Snow\_CCI project (Option 2; 2020-2022) advanced the multi-sensor multi-temporal algorithm to estimate the fractional snow cover (FSC). The current time series provides daily snow products of 5 km resolution with global coverage from 1 January 1982 until 30 June 2019. The snow product time series is a unique contribution to the climate community already making significant interest. The time series is one of the longest available, and there are no other such time series of daily and full coverage for both hemispheres. The novel multi-sensor multi-temporal algorithm has made this possible. Alternative time series have either much coarser resolution (due to the use of PMR data only) and are not able to cover the whole Earth on a daily basis (as optical data are limited by cloud cover and the polar night).

Keywords	Snow cover, climate monitoring, remote sensing
Target group	Climate and hydrological communities
Availability	Open
Project number	220 418 & 220 823 & 221 005
Research field	Earth Observation
Number of pages	38
© Copyright	Norsk Regnesentral & Project Teams



# Table of Content

<b>1</b>	<b>Introduction</b>	<b>7</b>
1.1	CryoClim cryospheric climate monitoring service	7
1.2	CryoClim global fractional snow cover product	7
<b>2</b>	<b>Satellite dataset</b>	<b>9</b>
2.1	Sensors	9
2.1.1	Optical sensors	9
2.1.2	Passive microwave radiometers	10
2.2	Dataset time series	11
<b>3</b>	<b>Retrieval algorithms</b>	<b>13</b>
3.1	Single-sensor algorithms	13
3.1.1	Optical algorithm	13
3.1.2	PMR algorithms	14
3.2	Multi-sensor multi-temporal algorithm	16
3.2.1	Hidden Markov model	16
3.2.2	Computing the optimal state sequence	18
3.2.3	Estimating FSC at 1%-precision level	19
3.2.4	Auxiliary data	21
3.3	Uncertainty estimation	21
3.3.1	Time interval to nearest cloud-free optical observation	22
3.3.2	Passive microwave surface temperature	22
3.3.3	Data log-likelihood for the no-snow state	22
3.3.4	Motivation of choice and algorithm	22
<b>4</b>	<b>Validation</b>	<b>24</b>
4.1	Validation with in-situ measurements	24
4.2	Validation with high-resolution satellite imagery	24
4.3	Validation results	25
<b>5</b>	<b>Product description</b>	<b>26</b>
5.1	Overall description	26

5.2	Time series characteristics.....	28
5.3	Known strengths and limitations.....	29
5.3.1	Strengths.....	29
5.3.2	Limitations.....	29
5.4	Product encoding.....	30
5.4.1	Snow cover extent (Layer 1).....	30
5.4.2	Uncertainty estimate (Layer 2).....	30
5.4.3	Land mask (Layer 3).....	31
5.4.4	Latitude (Layer 4).....	31
5.4.5	Longitude (Layer 5).....	31
5.5	Metadata description.....	31
5.6	Product format, storage and access.....	32
5.6.1	File format.....	32
5.6.2	File-name convention.....	33
5.6.3	Access.....	33
<b>6</b>	<b>References .....</b>	<b>34</b>

# 1 Introduction

Snow and land ice are key elements of the water cycle in countries at high latitudes and at high elevations. Seasonal snow is characterised by high temporal variability. At a short time scale the extent and properties of the snow cover are driven by meteorological events, so the year-to-year variability is also very high. The variations at daily-to-seasonal time scales are superimposed to long-term trends in the cryosphere, which have been observed during the last decades and are attributed to climate change (Lemke et al. 2007; Serreze et al. 2000).

The cryosphere is a critically important component of the Earth system, affecting the Earth's energy balance, sea level, greenhouse gases and atmospheric circulation, transport of heat through ocean circulation, ecology and human resource use and well-being (Callaghan et al. 2011). Due to the high spatial and temporal variability as well as inaccessible areas, satellite sensors are optimal tools for snow monitoring. Accurate observations of snow cover extent and physical properties are not only of interest for climate change research but are of great socio-economic importance.

## 1.1 CryoClim cryospheric climate monitoring service

The CryoClim project (2008-2013) developed a service for long-term systematic climate monitoring of the cryosphere (Solberg et al. 2014). The service provides sea ice and snow products of global coverage and glacier products covering Norway (mainland and Svalbard). The system and service is a contribution to the Global Earth Observation System of Systems (GEOSS) and the Global Cryosphere Watch (GCW) following the climate monitoring principles recommended by the Global Climate Observing System (GCOS).

CryoClim is an Internet service primarily based on satellite observations. The service is delivered through a web service and web portal ([www.cryoclim.net](http://www.cryoclim.net)). The portal includes manual searching, viewing and downloading capabilities. CryoClim is an operational and permanent service for long-term systematic climate monitoring of the cryosphere. The product production and the product repositories are hosted by mandated organisations. The databases are connected over the Internet in a seamless and scalable network, open for inclusion of more databases/sub-services.

## 1.2 CryoClim global fractional snow cover product

The CryoClim snow product was developed in the ESA/NoSA CryoClim project (2008-2013). It was a binary product mapping then snow cover extent (SCE). Algorithms were developed for single-sensor retrieval of the probability of SCE using optical and passive microwave radiometer (PMR) data. The probabilities were used in a novel multi-sensor multi-temporal fusion algorithm estimating the SCE (Solberg et al. 2015). The product was advanced in the ESA/NoSA Sentinel4CryoClim project (phase 1 and 2; 2015-2018) mitigating a number of initial weaknesses and adding uncertainty information (Solberg et al. 2018). The ESA Snow\_CCI project (Option 2; 2020-2022) advanced the multi-sensor multi-temporal algorithm to estimate the fractional snow cover (FSC) (Solberg et al. 2022). The current time series provides daily snow products of 5 km resolution with global coverage from 1 January 1982 until 30 June 2019. The snow

product time series is a unique contribution to the climate community already making significant interest. The time series is one of the longest available, and there are no other such time series of daily and full coverage for both hemispheres. The novel multi-sensor multi-temporal algorithm has made this possible. Alternative time series have either much coarser resolution (due to the use of PMR data only) and are not able to cover the whole Earth on a daily basis (as optical data are limited by cloud cover and the polar night).

The optical algorithm processes all available swaths from AVHRR GAC. The calculations are based on a Bayesian approach using a set of signatures (instrument channel combinations) and statistical coefficients. For each pixel of the swath, the probabilities for the surface classes *snow*, *bare ground* and *cloud* are estimated. The statistical coefficients are based on pre-knowledge of the typical behaviour of the surface classes in the various parts of the electromagnetic spectrum.

The algorithm for PMR is also based on a Bayesian estimation approach. For SSM/I and SSMIS four snow classes were defined in order to model the snow cover. For SMMR two classes were considered. The algorithm estimates the probability for each snow class given the PMR measurements. To improve the performance of the Bayesian algorithm, land cover data was included. This made it possible to construct a Bayesian estimator for each land cover regime.

The multi-sensor multi-temporal fusion algorithm (Rudjord et al. 2015; Solberg et al. 2018) is based on a Hidden Markov Model (HMM) simulating the snow states based on observations with PMR and optical sensors. The basic idea is to simulate the states the snow surface goes through during the snow season with a state model. The states are not directly observable, but the remote sensing observations give data describing the snow conditions, which are related to the snow states. The HMM solution represents not only a multi-sensor model but also a multi-temporal model. The sequence of states over time is conditioned to follow certain optimisation criteria. This approach was originally used to determine the binary snow cover extent (SCE).

In the most recent development (Solberg et al. 2022), the algorithm was advanced to estimate the fractional snow cover (FSC) down to the 1%-FSC level. This is done in two steps. First, more snow states were introduced to be able to estimate the snow cover in 10% categories. Second, we combined a histogram-equalisation approach and interpolation weighted by state probabilities to obtain 1%-FSC precision.

## 2 Satellite dataset

### 2.1 Sensors

#### 2.1.1 Optical sensors

The Advanced Very High Resolution Radiometer (AVHRR) sensor is carried on NOAA's Polar-orbiting Operational Environmental Satellites (POES) starting with TIROS-N in 1978 and on the MetOp series satellites owned and operated by EUMETSAT (Robel & Graumann 2014). On-board the TIROS-N, NOAA-6, 8 and 10 POES satellites, the AVHRR sensor measures in four spectral bands (AVHRR/1), while on the NOAA-7, 9, 11, 12 and 14 POES satellites, the sensor (AVHRR/2) measures in five bands. NOAA-7 AVHRR started service 24 August 1981. The AVHRR sensor on NOAA-15, 16, 17, 18 and 19 and on MetOp-A and MetOp-B measures in six bands, though only five are transmitted to the ground at any time (AVHRR/3). NOAA-15 AVHRR started service 13 May 1998.

AVHRR quantisation is 10 bits. The swath width is about 3000 km, and the spatial resolution is 1.1 km. Spectral features have been found that discriminate most clouds from snow and ground cover types.

AVHRR/3 channel 3 alternates during day and night between two wavelength intervals (3A during days and 3B during nights). The satellite provides coverage at least daily, and there are usually two satellites in orbit (morning and afternoon orbits).

Table 2.1: NOAA AVHRR/3 channels. AVHRR/1 did not include band 5, and AVHRR/2 missed band 3B.

Channel Number	Wavelengths [nm]
1	580-680
2	725-1000
3A	1580-1640
3B	3550-3930
4	10,300-11,300
5	11,500-12,500

AVHRR Level 1b data are grouped into four data types: HRPT (High Resolution Picture Transmission), LAC (Local Area Coverage), GAC (Global Area Coverage) and FRAC (Full Resolution Area Coverage). FRAC applies only to Metop satellites. GAC data are available globally since about 1978. The LAC and HRPT data types are most complete from 1985 forward and are limited to specific areas of the world. As a general rule, HRPT data are available for the U.S. and coastal areas and LAC data are available over foreign land masses. FRAC data is available for the entire globe since late October 2006.

For GAC data, successive sets of 4 out of every 5 samples in every third scan line are averaged to obtain an array of data spaced at intervals of 125 msec along the scan and at 500 msec along the satellite track. This leads to a data rate of 49,080 samples/minute and 2 scans/second. There are a total of 409 samples for the GAC data per channel per Earth scan.

### 2.1.2 Passive microwave radiometers

The scanning multichannel microwave radiometer (SMMR) was a five-frequency microwave radiometer flown on the Seasat and Nimbus 7 satellites (NSIDC SMMR 2018). Both were launched in 1978, with the Seasat mission lasting less than six months until failure. The Nimbus 7 SMMR lasted from 25 October 1978 until 20 August 1987. It measured dual-polarized microwave radiances at 6.63, 10.69, 18.0, 21.0, and 37.0 GHz (Table 2.2).

Table 2.2: SMMR channels and characteristics. (Njoku et al., 1980)

Channel Frequency [GHz]	Polarization	Half-power bandwidth [°]
6.6	V	4.56
6.6	H	4.51
10.69	V	2.93
10.69	H	2.91
18	V	1.80
18	H	1.81
21	V	1.50
21	H	1.49
37	V	0.93
37	H	0.93

The Special Sensor Microwave Imager (SSM/I) is a passive microwave radiometer flown aboard Defense Meteorological Satellite Program (DMSP) satellites (NSIDC SSM/I 2018). The DMSP orbit is near circular, sun synchronous and near polar, with an altitude of 860 km and an inclination of 98.8°. The orbital period is 102 minutes. This orbit provides complete coverage of the Earth, except for two small circular sectors 2.4° centred on the North and South poles (Wentz, 1988).

The SSM/I is a seven-channel total-power radiometer, which measures at four frequencies the linearly polarized microwave radiation emitted by the Earth-atmosphere system. Details concerning the radiometer setup can be found in Hollinger et al. (1987). Spatial resolutions vary with frequency (Table 2.3).

Table 2.3: SSM/I channels and antenna beamwidths. IFOV= instantaneous field of view, EFOV = effective field of view. The corresponding bands with same frequencies and polarizations were used with SSMIS, except for a substitution of SSM/I 85.5 GHz with SSMIS 91.665 GHz. (Hollinger et al. 1987)

Channel Frequency [GHz]	Polarization	Beam width IFOV [°]		EFOV on earth surface [km]	
		E-Plane	H-Plane	along-track	cross-track
19.35	V	1.86	1.93	69	43
19.35	H	1.88	1.93	69	43
22.235	V	1.60	1-83	50	50
37.0	V	1.0	1.27	37	28
37.0	H	1.0	1.31	37	29
85.5	V	0.41	0.60	15	13
85.5	H	0.41	0.60	15	13

The Special Sensor Microwave Imager / Sounder (SSMIS) combines and extends the imaging and sounding capabilities of three previously separate DMSP microwave sensors SSM/T-1 temperature sounder, the SSMI/T- 2 moisture sounder and the SSM/I. SSMIS is a 24-channel, 21-frequency, linearly polarized passive microwave radiometer system.

## 2.2 Dataset time series

The CryoClim multi-sensor multi-temporal algorithm fuses daily optical and PMR data. From the description of data sources above, we see that AVHRR/2 with five channels are available from 24 August 1981, while SMMR is available from 26 October 1978. Using AVHRR/1, a time series could be created from 1978. However, two thermal bands are essential for cloud detection, and in particular cloud detection over snow-covered surfaces. We have therefore chosen to start the time series from when the first full year of AVHRR/2 data is available, i.e. 1982.

As data sources we have used fundamental climate data records (FCDRs) for AVHRR and PMR provided by EUMETSAT Climate Monitoring Satellite Application Facility (CM SAF) ([www.cmsaf.eu](http://www.cmsaf.eu)). The AVHRR GAC data are described in Karlsson et al. 2016 (ATBD) and Karlsson et al. 2017 (documentation). The PMR data are described in Fennig 2017 (ATBD) and Fennig 2016 (documentation). During the first couple of decades of the time series there were periods of flaws due to sensor or satellite malfunctions. After around 2000 there were several sensors of each type in orbit making the acquisition system much more robust and giving better coverage in space and time.

The periods of PMR sensors are shown in Table 2.4, with emphasises on periods with flaws. To main versions of algorithms have been developed, one for SMMR and one for SSM/I. As the table shows, the 85 GHz channel failed for SSM/I on F8. We then switched to using the SMMR algorithm with corresponding and remaining SSM/I channels. Furthermore, the F10 satellite went into a flawed orbit and therefore delivered hardly usable data for an automated algorithm. We instead used F8 almost until F11 went into operation. In the period after F8 failure until F11 operation, we had to use F10.

Table 2.4: PMR time series with start and end dates of data used.

Satellite/sensor	Start date	End date	Algorithm	Comment
Nimbus 7 SMMR	25.10.1978	09.07.1987	SMMR algorithm	no 85 GHz channel
DMSP F8 SMM/I	09.07.1987	01.04.1988	SSM/I algorithm	fully operational
DMSP F8 SMM/I	01.04.1989	18.12.1991	SMMR algorithm	85 GHz channel failed
DMSP F10 SMM/I	18.12.1991	01.01.1992	SSM/I algorithm	larger errors due to elliptical orbit
DMSP F11 SMM/I	01.01.1992	?	SSM/I algorithm	
DMSP F13 SMM/I	24.03.1995	?	SSM/I algorithm	
DMSP F14 SMM/I	?	?	SSM/I algorithm	
DMSP F15 SMM/I	?	?	SSM/I algorithm	
DMSP F16 SMM/I	?	?	SSM/I algorithm	

DMSP F17 SMMIS	04.11.2006	?	SSM/I algorithm	85 GHz channel substituted with 91.7 GHz
DMSP F18 SMMIS	?	Present	SSM/I algorithm	85 GHz channel substituted with 91.7 GHz

The main issue with optical data has been sub-optimal acquisition time for NOAA 12 (low solar elevation due to orbital drift). The number of AVHRRs operating in orbit simultaneously has increased over time. Until 1998 there was only one AVHRR working at a time. From 13 May 1998, with the launch of NOAA 15, two sensors or more were operating on NOAA and more recently also MetOp satellites. This increased the spatial coverage substantially.

## 3 Retrieval algorithms

A description of the single-sensor (optical and passive microwave radiometer) and multi-sensor multi-temporal fusion algorithms are described in the following. The algorithm for uncertainty estimation is also described.

### 3.1 Single-sensor algorithms

A general solution for combining various data sources containing uncertain information is given by the Bayesian (inverse method) approach. Using this approach several measured variables can be combined to yield an optimal estimate. The approach is chosen here for single-sensor optical and passive microwave radiometer (PMR) data. It is based on prior knowledge of the relationship between each class and the satellite-measured variables. In addition, knowledge of the scatter of the expected measurement value for each class is needed. This knowledge is expressed as a probability density function (PDF) for the measurement variable given for the class.

Assume that we have  $n$  measured variables (may in general be vector observations)  $\mathbf{x}_1, \mathbf{x}_2, \dots, \mathbf{x}_n$ , that are independent, given a certain class (e.g., *snow*). A general expression is then derived for the probability of a class  $S_k$  given the measured variables:

$$P(S_k | \mathbf{x}_1, \mathbf{x}_2, \dots, \mathbf{x}_n) = \frac{p(\mathbf{x}_1 | S_k) \cdot p(\mathbf{x}_2 | S_k) \cdots p(\mathbf{x}_n | S_k) \cdot P(S_k)}{\sum_{m=1}^M p(\mathbf{x}_1 | S_m) \cdot p(\mathbf{x}_2 | S_m) \cdots p(\mathbf{x}_n | S_m) \cdot P(S_m)} \quad \text{Eq. 3.1}$$

The method works in such a way that the measurement, which gives the best discrimination between classes, is the one that gives most impact in the analysis. We do not only obtain an estimate of the most probable class, but also the uncertainty of this estimate. For all classes it is assumed that the features may be modelled as Gaussian distributions. It is further assumed that all features are uncorrelated, hence they are statistically independent under the Gaussian assumption.

#### 3.1.1 Optical algorithm

The optical snow cover algorithm is a probabilistic algorithm that was developed for AVHRR data. The algorithm estimates the probabilities for the surface classes snow, land and cloud using a set of combinations of satellite measurements ("features") together with statistical coefficients. The approach is based on prior knowledge of the relationship between each surface class and the satellite-measured variables. The relationship is described by the set of statistical coefficients.

The features are listed in Table 3.1 below. They are selected to exploit differences in the reflecting properties of the surface classes in various parts of the spectrum and to reduce variations with solar zenith angle. AVHRR channel 3A at 1.6 microns is particularly suited to discriminate snow and clouds, but this channel has only been available since 1998, and only on some of the platforms. When channel 3A is not available, AVHRR channel 3B at 3.7 microns is used instead. Channel 3B measures a combination of reflected sunlight and emitted thermal radiation. A method to estimate and subtract the thermal component is therefore used (Allen et al. 1990).

Table 3.1: Spectral features used in the optical algorithm.

Name	Description
A06	Reflectance at 0.63 microns (AVHRR channel 1)
R0906	Ratio of reflectance at 0.9 microns (AVHRR channel 2) to reflectance at 0.63 microns (AVHRR channel 1)
R1606	Ratio of reflectance at 1.6 microns (AVHRR channel 3A) to reflectance at 0.63 microns (AVHRR channel 1)
R3709	Ratio of reflectance at 3.7 microns (AVHRR channel 3B) to reflectance at 0.63 microns (AVHRR channel 1)
Tnwp-T10	Difference between the surface skin temperature from a numerical weather model and the 10.8 brightness temperature (AVHRR channel 4)

The static coefficients used by the algorithm are listed in Table 3.2 below.

Table 3.2: Static coefficients used in the optical snow cover algorithm.  
The spectral features are explained in Table 3.1.

Spectral feature	Snow		Land		Cloud	
	Mean	St. Dev.	Mean	St. Dev.	Mean	St. Dev.
A06	49.68	20.97	7.933	2.126	55.85	14.79
R0906	0.875	0.156	1.889	0.394	0.913	0.087
R1606	0.173	0.073	1.392	0.238	0.670	0.221
R3706	0.0273	0.026	0.369	0.117	0.190	0.133
Tnwp-T10	2.88	2.18	2.563	2.367	12.87	9.19

The swath products from one day are averaged and gridded into a daily product. A threshold is applied at 40% probability for cloud. If a pixel in the gridded product has the probability for the class cloud larger than 40% for all satellite passes during the aggregation period, the pixel is classified as cloud-covered in the final product. If there are one or more swath products during the aggregation period for which the probability for the class cloud is smaller than 40%, the probabilities for the classes snow and land are averaged. In this way the averaged probabilities for snow given cloud-free, and land given cloud-free are found. The probability for snow from the daily gridded product is used in the multi-sensor/multi-temporal algorithm.

### 3.1.2 PMR algorithms

The PMR approach estimates the probability for a set of classes given the PMR measurements. A set of features combining the PMR bands are calculated from the three types of sensors – SMMR, SSM/I and SSMIS.

For SSM/I and SSMIS four classes have been defined: *dry snow*, *wet snow*, *no-snow* and *snow with water* (a large fraction of open water in the observed pixel). Five features are applied ( $T$  denotes measured brightness temperature, the number denotes the frequency and  $h$  and  $v$  denote the polarization):

1. T37v - T37h
2. T19v - T37v
3. T22 - T85v

4.  $(1.95 \cdot T_{19v} - 0.95 \cdot T_{19h}) / 0.95$
5. T22

Feature 1 is applied by Grody & Bassist (1996) for detection of wet snow cover, Feature 2 and Feature 3 were used by Grody & Bassist (1996) for detection of dry snow cover, Feature 4 is an estimate of the surface temperature (Hiltbrunner & Mätzler 1997), and Feature 5 is used by (Grody & Bassist 1996) to eliminate precipitation.

Since the measured frequencies are different for SMMR (in particular the lack of 85 GHz), the SMMR features are different. As it is more difficult to estimate wet snow conditions, we consider only the two classes *snow* and *no-snow*. The retrieval algorithm apply two different features:

1.  $T_{18v} - T_{37v}$
2.  $T_{18h} - T_{37h}$

Feature 1 was suggested by Künzi et al. (1982) for detection of snow cover, while Feature 2 was suggested by Chang et al. (1987) for snow depth mapping. The polarization difference  $T_{37v} - T_{37h}$  feature where also considered, however, initial investigations showed poor performance with when using this feature for SMMR. It was therefore decided to use the gradient feature  $T_{18h} - T_{37h}$ .

The SCE estimator for SMMR is trained by using data from 73 Global Historical Climatology Network Daily (GHCND) stations, whereas the SCE estimator for SSM/I is trained using data from 32 Surface Synoptic Observations (SYNOP) stations. All selected meteorological stations are in the Northern Hemisphere.

Since the measured brightness temperature is not only dependent on the snow cover (and precipitation), but also the land cover, the algorithm takes land cover into consideration. For land cover data we use the GlobCover data set (Bicheron et al, 2008). The data includes 23 different land cover classes and information on the forest density. The Bayesian SCE estimator is constructed for different groups of land cover. For SMMR we consider the following 11 land cover groups:

1. Sparse vegetation and urban areas (land cover classes 150 and 190, respectively)
2. Open needle-leaved evergreen forest and open broad-leaved deciduous forest (land cover classes 90 and 60, respectively)
3. Mosaic forest or shrub land and mosaic grassland (land cover classes 110 and 120, respectively)
4. Closed to open broad-leaved evergreen forest and Closed broad-leaved deciduous forest (land cover classes 40 and 50, respectively).
5. Closed needle-leaved evergreen forest (land cover class 70)
6. Closed to open mixed broad-leaved and needle-leaved forest (land cover class 100)
7. Bare areas (land cover class 200)
8. Mosaic cropland and mosaic vegetation (land cover classes 20 and 30, respectively).
9. Closed to open shrub land (land cover class 130)

- 10. Close to open herbaceous vegetation (land cover class 140)
- 11. Rain-fed croplands and post-flooding or irrigated croplands (land cover classes 14 and 11, respectively).

For SSM/I we have merged the land cover groups 4, 5, & 6, and 8, 9 & 10 since the SYNOP stations does not cover all the land cover groups. Hence, for SSM/I we only consider 7 groups.

The SCE retrieval algorithm input is the PMR data, land cover data and PDFs for each class. If the most frequent land-cover class in the neighbourhood is *water body* (class 210), or land covers that are regularly or permanently flooded (class 160, 170 and 180), then the corresponding snow cover is set equal to zero. If the most frequent class is *permanent snow and ice* (class 220) then the snow cover is set equal to 100%. Otherwise, the class probabilities of each PMR observation is calculated for each swath. The probability swath data are then averaged over all observations that day and gridded, producing a daily snow probability.

### 3.2 Multi-sensor multi-temporal algorithm

The hidden Markov model (HMM) approach for the sensor fusion algorithm is described below.

#### 3.2.1 Hidden Markov model

Figure 3.1 shows the construction of a multi-sensor state model (right) from single-sensor state models (left). The optical model is more complex than the PMR model as fractional snow can be observed, which also makes it necessary to include states for temporary snow – giving a signal of temporary full snow cover properties.

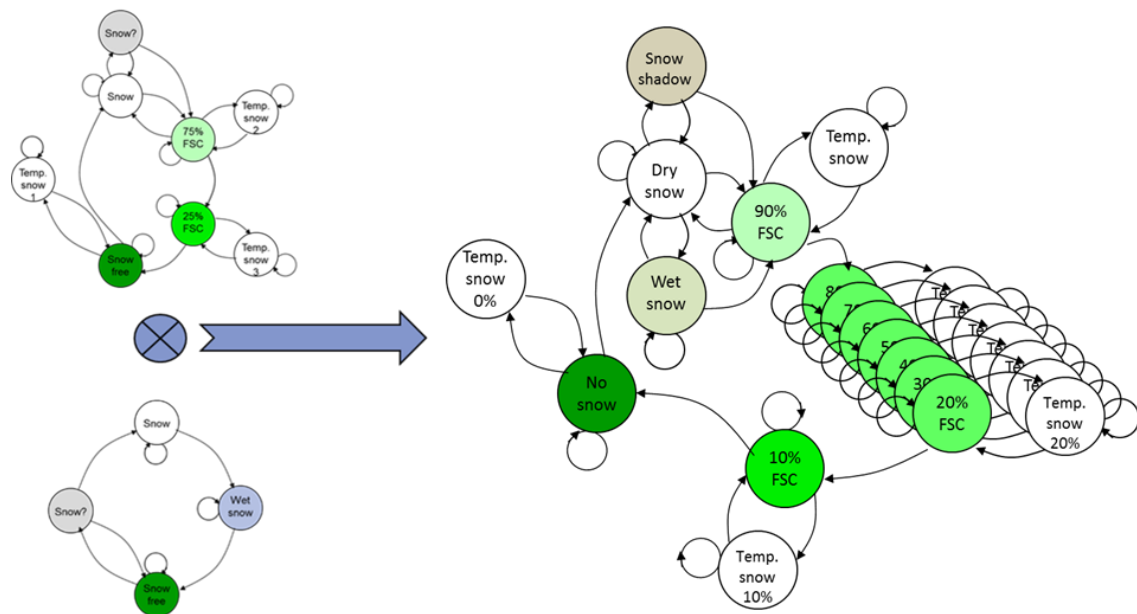


Figure 3.1: Single-sensor state model for optical (top left; original binary model) and PMR (lower left), and the new fused state model (right). The new model is a ten snow-cover categories model.

The model represents the following signatures:

- *Snow free*: No snow signature by either PMR or optical.
- *Temp. snow 1*: This is classified as snow by optical, but of low snow probability by PMR.
- *Snow*: This is a typical dry winter snowpack identified as snow by both optical and PMR.
- *Snow?*: This state is mainly intended to catch cloud shadows and other odd effects. Optical is expected to have a moderate snow signature with high uncertainty, while PMR shows high probability for snow.
- *Wet snow*: When the snow is wet, PMR often fails to detect it. This state has a low expected snow probability for PMR (and with high uncertainty). In optical, this is classified as snow.
- *FSC snow*: This indicates melting snow in the spring, where there are patches of bare ground appearing. The FSC values are in steps of 10% FSC with a range  $0\% < \text{FSC} < 100\%$  in optical, but with low expected snow signature for PMR (and also high uncertainty) due often wet snow.
- *Temp. snow for each FSC state*: These states represent precipitation of snow in the spring when the snow was previously melting. The snow might be dry for a short time but would normally quickly turn wet and melt away in a few days. This is seen as a strong snow signature in optical. In PMR the thin snow layer is assumed to be undetected.

In the following paragraphs we will describe the basic hidden Markov model (HMM) formalism (Baum et al. 1966). In an HMM we observe a system assumed to evolve through a series of different states. Transitions from one state to another happen with certain probabilities. While in a given state, the system will produce observables with a certain probability density. We will denote the set of discrete states  $Q$  of the internal system by:

$$Q = \{S_1, S_2, \dots, S_v\} \quad \text{Eq. 3.2}$$

where  $v$  is the number of states. Furthermore, the time series of observations,  $\bar{X}$ , will be denoted by:

$$\bar{X}^T = \{X^1, X^2, \dots, X^T\} \quad \text{Eq. 3.3}$$

where  $T$  is the number of elements of the sequence. The unknown state of the process at time  $t$  will be denoted  $E^t$ , thus  $E^t = S_i$  indicates that the process is in state  $S_i$  at time  $t$ . The states are not directly observable, but are related to observation  $X^t$  at time  $t$ , ( $t = 1, 2, \dots, T$ ) by a probability distribution of measurements:

$$p(X^t | E^t = S_i), i = 1, 2, \dots, v \quad \text{Eq. 3.4}$$

For a given time period, the model is also described by a set of transition probabilities between each pair of states:

$$p(E^t = S_i | E^{t-1} = S_j), i, j = 1, 2, \dots, v \quad \text{Eq. 3.5}$$

The probabilities of transition between the different states are obviously strongly dependent upon season, thus the process is not stationary, and the probabilities of transition are time dependent.

The final parameters of the model are the initial conditions defined by the probability of being in a given state at the initial time:

$$p(E^1 = S_i), i = 1, 2, \dots, v \quad \text{Eq. 3.6}$$

### 3.2.2 Computing the optimal state sequence

With a HMM, the notion of a class from the classification literature becomes the notion of a model in the HMM formalism. Traditionally, ground-cover classification in a temporal sequence of satellite images is the problem of assigning each grid cell in the scene to a class based on this cell's signal properties (or derived properties). In the HMM case, our aim is to assign each grid cell to the model that best explains the observed temporal evolution of the cell. Solutions to this kind of problem are important in many applications, and several algorithms are available. For our problem we have chosen to use the Viterbi algorithm.

The Viterbi algorithm is a dynamic-programming algorithm for finding the most likely sequence of hidden states (the Viterbi path) that results in a sequence of the observables. The Viterbi algorithm was proposed by Viterbi (1967) as a decoding algorithm for convolutional codes over noisy digital communication links. The algorithm requires as input the state probability density functions, the transition probabilities between the different states and the initial probability of each state.

Let  $V_{t,k}$  be the probability of the most likely state sequence responsible for the first  $t$  observations that has  $k$  as its final state, then:

$$V_{1,k} = p(X^1 | k) p(E^1 = S_k) \quad \text{Eq. 3.7}$$

$$V_{t,k} = p(X^t | k) \max_i (p(E^t = S_i | E^{t-1} = S_j) V_{t-1,k}) \quad \text{Eq. 3.8}$$

The Viterbi path can be retrieved by saving back pointers that remember which state  $i$  was used in the second equation.

The algorithm takes as input three sets of probabilities, the initial probabilities,  $\pi_i$ , of each state,  $S_i$ , the transition probabilities,  $a_{ij}$ , between two states,  $S_i$  and  $S_j$ , and the probabilities,  $b_i(X^t)$ , of each state  $S_i$  given the observation,  $X^t$ .

Let  $V_{t,k}$  be the probability of the most likely state sequence responsible for the first  $t$  observations that has  $k$  as a final state, and let  $\psi^t(S_k)$  be the most probable state,  $S_i$ , at time  $t - 1$ , given that the state at time  $t$  is  $S_k$ .

The Viterbi algorithm consists of four parts in order to find the most likely sequence:

1. *Initialisation*: The probabilities  $V_{1,k}$  for the different states,  $k$ , at the first step in the path are derived from the initial probabilities and the observations, and can be stated as  $V_{1,k} = b_k(X^1)\pi_k$
2. *Recursion*: For each following step ( $2 \leq t \leq T$ ) in the sequence, the probability for each of the states,  $k$ , can be found recursively from the existing path of probabilities and transition probabilities:  $V_{t,k} = \max_{1 \leq i \leq v} [V_{t-1,i}a_{ki}]b_k(X^t)$ . Likewise, the most probable of the states at the *previous* time step  $t - 1$  for each of the possible *current* states  $S_k$  at time  $t$ , is determined as:  
 $\psi^t(S_k) = \operatorname{argmax}_{1 \leq i \leq v} [V_{t-1,i}a_{ki}]$ .
3. *Termination*: At the final time step,  $T$ , the most probable state is selected:  $S_{T\max} = \operatorname{argmax}_{1 \leq i \leq v} [V_{T,i}]$  with its corresponding probability  $P_{\max} = \max_{1 \leq i \leq v} [V_{T,i}]$ .
4. *Sequence backtracking*: Finally, the algorithm iterates through the steps backwards and selects the optimal sequence of states  $S_{t\max}$  from the calculated probabilities:  $S_{t\max} = \psi^{t+1}(S_{t+1\max})$

For the snow maps, the sequences corresponding to each pixel are done in parallel. Initialization is done for the first map in the dataset, and then the recursion is performed for each following map. At each step  $t$ , a map containing the most probable state  $\psi^t(S_k)$  at the previous step  $t-1$ , for each of the possible current states  $S_k$  is written to file. The corresponding logarithm of the probabilities ( $\log[V_{t,k}]$ ) are also written to a temporary file. Logarithms are used to minimize numerical errors, due to the vast range of possible probabilities involved.

For the last snow map in the time series, the termination is performed. The final state with the highest accumulated probability, is found. Finally, the backtracking is performed. The algorithm iterates backwards through the dataset and selects the most likely state for every pixel at each time step.

The result is the most probable time series of states for each grid cell in the product. This gives a product showing the estimated snow state in each grid cell. The states are then assigned “Snow”, “Snow free” or corresponding 10% FSC category.

### 3.2.3 Estimating FSC at 1%-precision level

From this model, an algorithm is developed to estimate FSC with a resolution of 1% by averaging over several states. Using the HMM with 10% resolution and the Viterbi algorithm, a snow state is found for each time step as described above. This will in the following be referred to as the *primary* state. Furthermore, a *secondary* state is also found for each time step. This is found by the following additions to the Viterbi algorithm:

- In step 2 (*Recursion*), the *second* most probable state,  $\psi_s^t(S_k)$ , at the *previous* time step  $t - 1$  for each of the possible *current* states,  $S_k$ , at time  $t$ , is also found, as follows  $\psi_s^t(S_k) = \operatorname{argmax}_{1 \leq i \leq v, i \neq imax} [V_{t-1,i}a_{ki}]$ . Here *imax* is the index found previously, giving the most likely state.

- In step 3 (*Termination*), the second most probable state is also selected,  $S_{T_{max,s}} = \operatorname{argmax}_{1 \leq i \leq v, i \neq i_{max}} [V_{t,i}]$ , with its corresponding probability  $P_{max,s} = \max_{1 \leq i \leq v, i \neq i_{max}} [V_{t,i}]$ . This is the secondary state for the final time step,  $T$ .
- In step 4, during *sequence backtracking*, the algorithm also selects the second most probable state,  $S_{t_{max,s}}$  for each time step in the sequence based on the calculated probabilities:  $S_{t_{max,s}} = \psi_s^{t+1}(S_{t+1_{max}})$ .

If the primary state is found to be in one of the states of either full snow cover, or a snow-free state, the secondary state is ignored. The secondary states are only used together with the primary states when the primary state for a given time step is one of the partial snow cover states,  $0\% < \text{FSC} < 100\%$ , or one of the corresponding states for *temp. snow*. In these cases, the FSC estimate is found as the average of the FSC of these two states, where the probabilities of the states are used as weights, as follows:

$$FSC_t = [P_{max,s} FSC(S_{t_{max,s}}) + P_{max} FSC(S_{t_{max}})] / (P_{max,s} + P_{max}) \quad \text{Eq. 3.9}$$

The optical and PMR snow probabilities are input to the multi-sensor/multi-temporal algorithm. The data probabilities,  $b_i(X^t)$ , of each state,  $S_i$ , given the observation  $X^t$ , are found assuming a multivariate distribution (see Solberg et al. 2018 for details).

The original algorithm used a Gaussian multivariate distribution. However, when interpolating between primary and secondary states, this is no longer suitable. Due to the shape of the Gaussian distribution, the primary state would have a considerably higher probability than the secondary state and would therefore dominate the FSC estimate. This would cause certain FSC values to be considerably overrepresented.

Student's t-distribution has a more slowly diminishing tail, and therefore provides more even balance between the primary and secondary states. It is found that using this distribution with five degrees of freedom ( $v = 5$ ), a more realistic distribution of FSC estimates is obtained.

The distribution of FSC values still contains some artifacts, however. Physically, we expect that the FSC values for partial snow cover (i.e., excluding full snow cover, 100%, and bare ground, 0%), should be relatively evenly distributed. The pattern we see is increasing values up to a peak exactly every 10% of FSC. This repeating pattern is artificial, and matches the intervals used in the algorithm. We therefore performed a histogram transformation to reduce this artifact in the data.

We used a histogram equalization to flatten the histogram, making it closer to uniform. As we want to compensate for these artifacts only, and not real variations in FSC distributions, we based the transformation on the repeating pattern. Each interval 1-10, 21-30, etc. was transformed separately.

The transform was trained on all the FSC products from the Northern Hemisphere from three years over a twenty-year period. In order to transform any float value, an

analytical expression of the transform was found. A 3<sup>rd</sup> degree polynomial was fit to the cumulative histogram, giving coefficients

$$c_0 = -0.866015, c_1 = 0.988041, c_2 = -0.213079, c_3 = 0.0212775$$

The transformed FSC values were then found from the original FSC values the following way:

1. Transform to the short segment:  $x = (FSC - 1) \bmod 10 + 1.5$
2. Perform histogram equalization:  $y = c_3x^3 + c_2x^2 + c_1x + c_0$
3. Transform back to FSC values:  $FSC_{new} = y + FSC - x$

Since this is intended as a transform to equalize FSC values for partial snow cover, FSC values of 0% and 100% are not transformed.

### 3.2.4 Auxiliary data

The classification of PMR data is stratified into different land cover types as the measured brightness temperature is not only dependent on the snow cover (and precipitation), but also the land cover. The algorithm takes the land cover into consideration. For land cover data, we use the GlobCover data set (Bicheron et al. 2008). The data includes 23 different land-cover classes and information on the forest density. The Bayesian SCE estimator is constructed for different groups of land cover.

A land mask is applied for retrieval of FSC, which specifies the exact domain for retrieval. The mask represents the actual land area with areas of land ice removed. Lakes smaller than the 300 m in extent have also been removed in the original data. Resampling to 5 km spatial resolution removed water bodies of extent less than 5 km. The source of the land, waterbody and land ice masks is GlobCover version 2.2 used (Bicheron et al. 2008).

The optical algorithm needs model surface temperature from numerical weather prediction. The model surface temperature (skin temperature) is used in combination with brightness temperature measured at 10.8 microns (AVHRR channel 4) as the fourth measured feature in the algorithm (Table 3.1). When processing AVHRR GAC data for 1982–2019, the model surface temperature is collected from ECMWF ERA interim. The model temperature is interpolated into the satellite swath grid using linear interpolation in time and space. A precise model temperature is essential for the fourth feature (Tnwp-T10) to correctly identify cold clouds. If the gap between the real temperature and the interpolated modelled temperature becomes too large, this may push the algorithm towards erroneous classification.

### 3.3 Uncertainty estimation

The uncertainty is estimated using a logistic regression analysis, where the independent variables are the time interval to nearest cloud-free optical observation, the surface temperature (estimated from PMR data), and the average data log-

likelihood of the snow states. The target variables are status of the decision of our FSC algorithm, correct or incorrect, validated by in-situ measurements.

### 3.3.1 Time interval to nearest cloud-free optical observation

In general, the optical sensors provide more reliable data for estimating the FSC than a passive microwave radiometers (PMR). However, under cloudy conditions we only have the PMR data available.

In previous work (Solberg et al. 2018), we noticed that the accuracy decreases when the time to/from the next/last cloud-free optical observation increases. The trend is not as clear for this product, where we observe no clear correspondence between the RMSE and the time to optical observation.

### 3.3.2 Passive microwave surface temperature

For SSM/I, an estimate of the surface temperature is given as

$$T = \frac{1.95 \cdot T_{19v} - 0.95T_{19h}}{0.95} \quad \text{Eq. 3.10}$$

where  $T_{19v}$  and  $T_{19h}$  denotes measured brightness temperature at 19 GHz for vertical and horizontal polarizations, respectively. For the SMMR sensor, we apply the corresponding 18 GHz brightness temperatures.

From previous exploratory data analysis (Solberg et al. 2018), we observed that the accuracy was lower for surface temperature between about 0 and 20°C with a minimum at 16°C. A similar observation was observed for AVHRR in the Snow\_CCI project, where the RMSE of the FSC was highest for a brightness temperature (band 4) of 2°C. For this product, we observe a decreasing RMSE for increasing surface temperature up to about 300 K. For temperatures above 300 K the RMSE is zero.

### 3.3.3 Data log-likelihood for the no-snow state

In the Snow\_CCI AVHRR product uncertainty layer, we observed a correlation between the band 1, band 3b and the solar incidence angle, in addition to band 4. For CryoClim FSC, the AVHRR data may not be available at the corresponding date and location due to cloud conditions.

In the CryoClim SCE binary product, we noticed that the average data log-likelihood of the snow states is a measure of uncertainty. A similar dependence was observed here. The RMSE decreases for increasing data log-likelihood values of the no-snow state.

The independent variables are based on the surface temperature, the time interval to nearest cloud-free optical observation, and the data log-likelihood for the no-snow state. However, similar to AVHRR in the Snow\_CCI baseline project, we estimate the RMSE of the FSC, and establish the logistic regression model using reference data extracted from Landsat data of much higher resolution.

### 3.3.4 Motivation of choice and algorithm

A systematic error-analysis approach was selected and applied. A key observation from the Snow\_CCI baseline project exploratory data analysis (EDA) was that the

statistical error (computed using error propagation) contributed little to the RMSE, and for some features, the modelled statistical error was larger than the observed RMSE. The systematic error more or less constituted the whole RMSE.

Since the RMSE is bound by 0 and 100, we estimate the RMSE using a logistic regression approach. We assume that squared error (RMSE) for the  $i$ th pixel follows a binomial distribution with an  $n$  parameter equal to 100. The expectation of a binomial random variable  $X_i$  is given by  $E[X_i] = p_i$ . Using a generalized linear model (GLM) with a logit link function  $g(\mu_i) \triangleq \eta_i = \log p_i / (1 - p_i)$ , where  $\mu_i = E[X_i]$ .

In general, for a set of independent variables  $f_i^1, f_i^2, \dots, f_i^N$ , we model  $\eta_i$  as

$$\eta_i = a_0 + a_1 \cdot f_i^1 + a_2 \cdot f_i^2 + \dots + a_N \cdot f_i^N. \quad \text{Eq. 3.11}$$

From these equations, the pixel-wise RMSE is estimated as

$$RMSE = \frac{\exp(\eta)}{1 + \exp(\eta)}. \quad \text{Eq. 3.12}$$

To evaluate the goodness of the approach, we perform cross-validation over the 186 Landsat images that constitute the reference data. Hence, we leave one reference image out, estimate the model from the remaining 185 reference images, and predict the RMSE for each pixel in the hold-out reference image. Finally, we compute the average “ground truth” RMSE and average predict RMSE for the hold-out reference image and plot the values. In this cross-validation experiment, the RMSE and bias of the estimated RMSE is 15.6 and 0.07 respectively, and the  $R^2$  is 0.16. We also note that the ground truth RMSE are very high for some images.

The RMSE for CryoClim FSC will be estimated as:

$$\eta = 15.05 - 0.051 \cdot ll_s + 0.019 \cdot |d| - 0.061 \cdot T \quad \text{Eq. 3.13}$$

where  $T$  is the surface temperature estimated by the PMR data,  $|d|$  is the time interval to nearest cloud-free optical observation and  $ll_s$  is the data log-likelihood of the no-snow states.

## 4 Validation

The validation of the Snow\_CCI OP-2 CryoClim FSC product and corresponding uncertainty estimates, served two overall objectives:

1. Study performance of the new CryoClim FSC product relative to the previous CryoClim SCE v. 2.0 binary product.
2. Study performance of the new CryoClim FSC product with respect to the Snow\_CCI baseline project.

The first objective was to ensure that the new FSC product has similar performance as the previous SCE binary product after the development of the modified retrieval model for the algorithm to handle FSC. It also serves as documentation of the overall performance compared to previous versions of the CryoClim product.

The second objective is driven by the goals of the Snow\_CCI project using the same dataset as the baseline project to analyse and document the relative performance of the new CryoClim FSC product compared to the other FSC products in the Snow\_CCI baseline project.

### 4.1 Validation with in-situ measurements

The quality of the CryoClim FSC product has been validated in different areas of varying topography and land use. Ground-based measurements (in-situ data) are an excellent source but represents usually only information for a certain point. High-resolution optical satellite data with its greater spatial coverage can fill the gap between point measurements and coarser resolution products.

Four datasets are suitable for the purpose of validation against in-situ data. The Global Historical Climatology Network - Daily (GHCN-D) dataset (Menne et al. 2012) was used initially in the CryoClim project and was in the Sentinel4CryoClim project extended and refined. Furthermore, we used the, by several authors in the snow research community, recommended high-quality datasets from the former Soviet Union (see, e.g., Brun et al. 2013). These are the Historical Soviet Daily Snow Dataset (HSDSD) Version 2 dataset (Armstrong 2001), the Former Soviet Union Hydrological Snow Surveys (FSUHSS) dataset (Krenke 2004) and Snow Cover Characteristics from Russian Meteorological Stations and from some meteorological station over the Former USSR provided by RIHMI-WDC (RHIMI) (Bulygina et al. 2010).

### 4.2 Validation with high-resolution satellite imagery

Snow reference data derived from Landsat sensors (Thematic Mapper family) and Sentinel-2 (Multispectra Imager) offers excellent resolution and spectral information to generate high-resolution reference snow maps. A validation dataset based on Landsat data was prepared in the Snow\_CCI baseline project. This dataset has also been used for validation of the CryoClim FSC product. All reference snow maps were re-projected in the geographic map projection on WGS84 ellipsoid and aggregated to a fractional snow cover extent at the resolution of  $0.05^\circ$ . For characterising the results of the pixel-

by-pixel inter-comparison, the statistical measures bias, root mean square error (RMSE), unbiased RMSE and cross-correlation are used.

### **4.3 Validation results**

The validation based on in-situ data shows that the accuracy of the FSC product varies by year and season. Yearly overall accuracy is found to be mostly between 90 and 94%, with some exceptions. The seasonal variation in accuracy is stronger, giving monthly accuracies between 85 and 100% for the year 2014.

Based on in-situ data, the CryoClim FSC product and the CryoClim SCE v. 2.0 binary product show very comparable results. The overall accuracy of the two products is similar. There are, however, some differences in trends, as the binary product performs better in the period using PMR data from the SMMR sensor, while the FSC product performs better in the period using the SSM/I F8 sensor. The reason for this difference is unclear. The seasonal trends for the two products appear comparable.

The validation using high-resolution satellite imagery was based on 543 high-resolution (HR) Landsat scenes where snow maps were derived by three different retrieval algorithms. The CryoClim FSC product was compared with the HR-derived snow maps in FSC product resolution. CryoClim FSC represents snow on ground (SCFG). The overall accuracy is high showing an RMSE in the order of 16% and a bias lower than 2.4%. Separating open and forested areas, show very good performance in open areas (13-14% RMSE), and also quite good results for forested areas (17-18% RMSE). When considering FSC aggregated in steps of 10%, a tendency to overestimate the SCF for higher values was found, including an increase of the RMSE.

For the validation of CryoClim FSC uncertainty estimates, a general overestimation of the uncertainty of 2-3% was found. The RMSE was around 15%, indicating a large variance of the error in the provided uncertainty layer.

## 5 Product description

The overall aim of the CryoClim fractional snow cover (FSC) climate data record is to provide one of the longest snow cover extent time series available with global coverage and without hindrance from clouds and polar night. This has been achieved by utilising the best features of optical and passive microwave radiometer (PMR) observations of snow using a sensor-fusion algorithm generating a consistent time series of global FSC products (Solberg et al. 2014, 2015, 2018, 2022; Rudjord et al. 2015).

### 5.1 Overall description

AVHRR sensors aboard the satellites NOAA-7, -9, -11, -14, -16, -18, -19 have been used as the optical data source, and SMMR aboard the Nimbus 7 satellite, and SSM/I and SSMIS sensors aboard the DMSP F8, DMSP F11, DMSP F13, DMSP F14, DMSP F15, DMSP F16, DMSP F17 and DMSP F18 satellites, respectively, have been used as PMR data source. The CryoClim multi-sensor multi-temporal concept for fusion of optical and PMR data for retrieval of FSC is based on a hidden Markov model (HMM) where 10%-level FSC states are modelled. The last part of the algorithm carries out a weighted interpolation between 10%-FSC states to reach 1%-FSC precision.

The FSC product represents snow cover on the ground and is processed in a 5 km grid resolution and finally projected to a latitude/longitude grid of 0.05° resolution (Table 5.1). The time series characteristics are provided in Table 3.1. A product example is provided in Figure 5.1 (FSC) and Figure 5.2 (associated uncertainty). There are no data gaps in the time series. However, there are periods of reduced product quality due to sensor problems or missing data in the 1980s and 1990s (Table 5.2, Table 5.3).

Table 5.1: CryoClim FSC time series characteristics.

<i>Subject</i>	<i>CryoClim Fractional Snow Cover CRDP prototype version</i>
Variable	Fractional snow cover [%]
Accuracy target	10-20% unbiased RMSE
Retrieval algorithm	Solberg et al. 2014, 2015, 2018, 2022; Rudjord et al. 2015; adapted from binary to FSC
Uncertainty algorithm	Salberg et al. 2022
Satellite(s)	NOAA-7, -9, -11, -14, -16, -18, -19; Nimbus-7, DMSP F8, - F10, - F11, - F13, - F14, - F15, - F16, - F17 and - F18
Sensor(s)	AVHRR, SMMR, SSM/I and SSMIS
Input product(s)	Level-1B FCDRs from EUMETSAT CM SAF
Geographical domain(s)	Global
Start date time series	01.01.1982
End date time series	30.06.2019
Grid size	5 km
Projection/datum	EASE Grid 2.1 / WGS 84
Temporal resolution	Daily
Temporal aggregation	None
Number of layers	5

Subject	<i>CryoClim Fractional Snow Cover CRDP prototype version</i>
Metadata	Global attributes in NetCDF4 file, CF-v1.9, conformal with CCI data standards v2.3, 26/07/2021
Auxiliary data	The source of the land, waterbody and land ice masks is GlobCover version 2.2 (Bicheron et al. 2008). Historical model temperature data from ERA-Interim global atmospheric reanalysis (Dee et al. 2011) is used to cover the optical snow cover algorithm's need for model surface temperature data
Data representation	Unsigned byte (8 bits)
File format	NetCDF4, CF-v1.9
Product access	<a href="http://www.cryoclim.net">www.cryoclim.net</a>

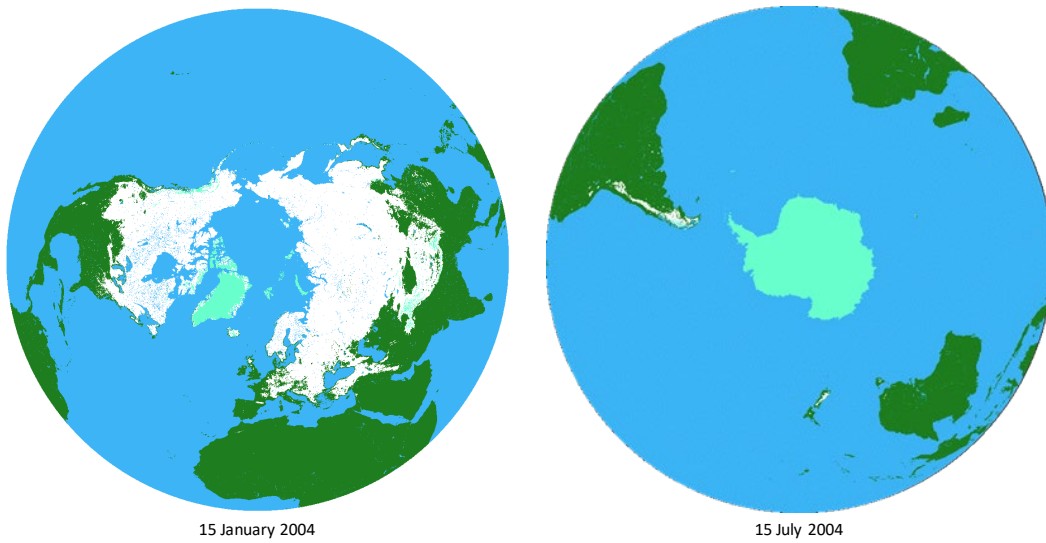


Figure 5.1: Example of daily fractional snow cover (FSC) maps for Northern Hemisphere on 15 January 2004 (left) and Southern Hemisphere on 15 July 2004 (right).

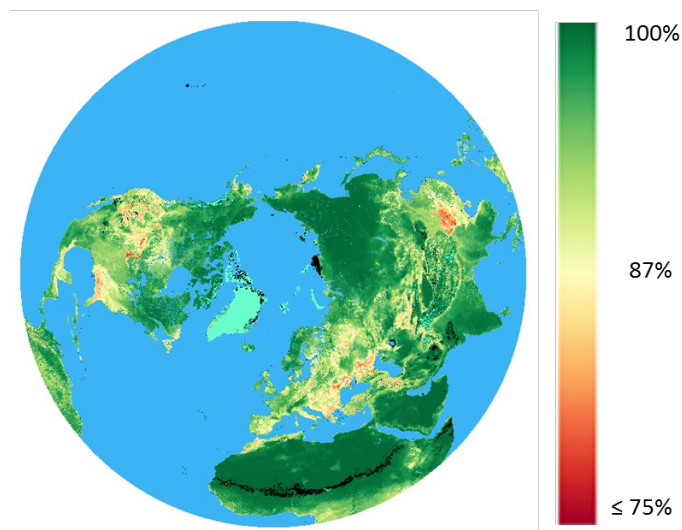


Figure 5.2: Example of a SCE retrieval uncertainty map for 27 February 2004.

## 5.2 Time series characteristics

The periods of reduced product quality are briefly explained in the following (Table 5.2). Biases associated with Nimbus 7 SMMR and DMSP F-8 SSM/I have been observed, in particular in the summer period with almost only wet and patchy snow present.

SMMR did not have the 85 GHz channel and had a somewhat different set of channel frequencies. The 85 GHz channel on the first SSM/I instrument failed early in the mission. The lack of 85 GHz channels on both satellites and the channel differences between the instruments have resulted in somewhat variable retrieval algorithm performance. A tailored algorithm is used with data from Nimbus 7 and DMSP F-8. However, the performance deviate from that of the algorithm we use with other SSM/I and SSMIS instruments. A positive bias appears in the retrieval results, and it is largest for DMSP F8. The problem seems to be associated with patchy (and probably wet) snow cover. The bias seems to be most pronounced in the summer season. We recommend caution for regions of patchy/wet snow in the summer period for the years 1982-1991.

There are periods of unfavourable illumination conditions with the early NOAA satellites. The NOAA satellites do not include any system to stabilise their orbit, resulting in orbital drift and therefore acquisitions progressively earlier (for morning satellites) and later (for afternoon satellites). At very low solar angles, the discrimination power of the optical retrieval algorithm is reduced, resulting in more mixture between snow and clouds. The problem is most prominent when data from only one satellite is available (in particular NOAA-12). When more satellites became available and satellites were launched into an orbit with equatorial passage time closer to noon in the late 1990s, the problem became less pronounced. In the last 20 years there has been more redundancy (more sensors in orbit) and therefore no periods of reduced quality.

Table 5.2: Periods of reduced product quality in the CryoClim FSC time series.

Start date	End date	Reason
01.01.1982	09.07.1987	Reduced discrimination power due to fewer channels on Nimbus 7 SMMR
01.04.1989	18.12.1991	Loss of 85.5 GHz channel DMSP F8 SSM/I
18.12.1991	01.01.1992	Larger acquisition errors due to elliptical orbit
14.09.1994	19.01.1995	Unfavourable illumination conditions due to dependency on NOAA 12 only

For the whole time series, there are 27 days with neither optical nor PMR retrieval (Table 5.3). These are individual days and not series of days in a row. The multi-sensor time-series algorithm handles this by making a best estimate of snow cover, based on days both prior to and following after the lack of data. This will not reduce the quality of the snow maps much for days without data as long as they are just individual days.

Table 5.3: List of days with no input data (neither optical nor PMR for either hemisphere).

Dates with no satellite data			
19820529	19830806	19841206	19850216
19820531	19830921	19850204	19850218
19820926	19830923	19850206	19850220
19830727	19830925	19850208	19850222
19830729	19840115	19850210	19850224
19830731	19840410	19850212	19860315
19830802	19840723	19850214	

The algorithm estimating the uncertainty associated with the FSC maps needs observations of covariates from the same day as the time stamp of the FSC product. These covariates are partly based on data from PMR sensors. Hence, estimates of uncertainty could not be produced for days lacking PMR acquisitions (Table 5.4).

Table 5.4: Overview over days per year with no uncertainty estimate for either hemisphere.

Year	Number of days without uncertainty estimate
1982	5
1983	14
1984	5
1985	22
1986	1
1988	6
2008	2

## 5.3 Known strengths and limitations

### 5.3.1 Strengths

The product provides the fraction of snow cover on the ground per grid cell on global land areas, except for glaciers. The data record provides one of the longest snow cover time series available with global coverage and without hindrance from clouds and polar night on a daily temporal resolution. The spatial resolution of the product, 5 × 5 km grid size, is high compared to other available satellite-based global snow products providing full spatial coverage on a daily basis year around (i.e. also for areas covered by clouds and polar night), which are all based on PMR data only of typically 10-25 km resolution. The product provides snow on the ground, compensating potential obstructed view from vegetation canopy. The product quality is high, as validation results gave an overall accuracy with an RMSE in the order of 16% and a bias lower than 2.4%. The product comes with uncertainty estimates on the grid-cell level.

### 5.3.2 Limitations

The quality of the input data was not optimal all through the first two decades of the time series due to sensor limitations, sensor-band failures and orbital drift of satellites. Biases associated with Nimbus 7 SMMR and DMSP F-8 SSM/I have been observed, in particular in the summer period with almost only wet and patchy snow present. SMMR

did not have the 85 GHz channel, and the channel failed on DMSP F-8 after a period. The bias seems to be most pronounced in the summer season. We therefore recommended caution for regions of patchy/wet snow in the summer period for the years 1982-1991. There are periods of unfavourable illumination conditions with the early NOAA satellites due to orbital drift and less favourable passage timing over time. The problem is most prominent when data from only one satellite is available (in particular for NOAA-12). When more satellites became available and satellites were launched into an orbit with equatorial passage time closer to noon in the late 1990s, the problem became less pronounced. In the last 25 years or so there has been more redundancy (more sensors in orbit) and therefore no periods of reduced quality.

## 5.4 Product encoding

The product is composed of five layers, which are described in the following.

### 5.4.1 Snow cover extent (Layer 1)

The thematic content is snow cover extent (SCE) per grid cell retrieved by the multi-sensor multi-temporal algorithm. The snow cover is described by categorical values representing binary snow cover (snow/no-snow). The effective fractional snow cover (FSC) threshold is aimed to be close to 50%. Even if the algorithm aggregates data throughout the day, the map is intended as an estimate of the snow situation at noon. Values are represented as **16 bits signed integer**. The encoding scheme applied for snow and other map categories are explained in Table 5.5 together with the colour table values applied in the map example.

Table 5.5: The encoding scheme for Layer 1 and suggested colour table values for visualisation.

Code	Description	R	G	B	Colour
0	No data	0	0	0	
41	Water body	60	180	245	
43	Land ice	105	255	205	
100-125	FSC = 0-25%	4	130	4	
126-150	FSC = 26-50%	86	171	86	
151-175	FSC = 51-75%	170	212	170	
176-200	FSC = 76-100%	254	254	254	

### 5.4.2 Uncertainty estimate (Layer 2)

The content is uncertainty estimate of the retrieved FSC per grid cell. Values represent the estimated root mean square error (RMSE). The range of RSME is 0.0 – 1.0. **Values are represented as 32 bits floating point**. The encoding scheme applied is explained in

Table 5.6.

Table 5.6: The encoding scheme for Layer 2 and suggested colour table values for visualisation. Note that water body and land ice are retrieved from Layer 1 (SCE).

Code	Description	R	G	B	Colour
-1	No uncertainty estimate	0	0	0	
41	Water body	60	180	245	

43	Land ice	105	255	205	
100-105	RMSE = 0.0-5.0% FSC	1	106	56	
106-110	RMSE = 5.6-10.0% FSC	135	203	103	
111-115	RMSE = 10.1-15.0% FSC	253	199	118	
116-120	RMSE = 15.1-20.0% FSC	165	110	60	
121-125	RMSE = 20.1-25.0% FSC	165	75	60	
>125	RMSE > 25.0% FSC	165	0	38	

### 5.4.3 Land mask (Layer 3)

The land mask applied for retrieval of SCE, which documents the exact domain for SCE retrieval. The mask represents the actual land area with areas of land ice removed. Lakes smaller than the 300 m in extent have also been removed in the original data. Resampling to 5 km spatial resolution removed water bodies of extent less than 5 km. The source of the land, waterbody and land ice masks is GlobCover version 2.2 used (Bicheron et al. 2008). Values are represented as 8 bits unsigned integer.

### 5.4.4 Latitude (Layer 4)

Latitude for each grid cell in the product. Values are represented as 32 bits floating point. The coordinate values represent the centre position in the product grid.

### 5.4.5 Longitude (Layer 5)

Longitude for each grid cell in the product. Values are represented as 32 bits floating point. The coordinate values represent the centre position in the product grid.

## 5.5 Metadata description

The metadata are according to the netCDF CF convention (version 1.4). The conventions define metadata that provide a definitive description of what the data in each variable represents, and the spatial and temporal properties of the data. The data are included in the same file as the data, thus making the file "self-describing". The global attributes are listed in Table 5.7.

Table 5.7: NetCDF CF global attributes for a product from the Southern Hemisphere.

Name	Value
title	Snow cover for Southern Hemisphere
southernmost_latitude	-90.0 [float value]
northernmost_latitude	0.0 [float value]
westernmost_longitude	-179.968 [float value]
eastermost_longitude	180.0 [float value]
area	Southern Hemisphere
projection	ease
resolution	5.0 km
source	NA
institution	Norwegian Computing Center
history	2019-01-05 creation
conventions	CF-1.4

PI_name	CryoClim Snow and Ice Manager
abstract	Binary snow cover prototype product estimated from optical and passive microwave satellite data for the CryoClim project
activity_type	Space borne instrument
contact	cryoclim@met.no
distribution_statement	Free
keywords	Snow Cover, Terrestrial Snow, Oceanography, Meteorology, Climate, Remote Sensing
product_name	cryoclim_snow_cover_reproc
project_name	CryoClim
start_date	2004-01-01 00:00:00
stop_date	2004-01-02 00:00:00
topiccategory	Climatology Meteorology Atmosphere
gcmd_keywords	Cryosphere > Snow/Ice > Snow Cover, Terrestrial Hydrosphere > Snow/Ice > Snow Cover, AVHRR > Advanced Very High Resolution Radiometer, SSM/I > Special Sensor Microwave Imager

## 5.6 Product format, storage and access

The file format of the product, product file name convention and product access are explained in the following.

### 5.6.1 File format

The product is stored in the Network Common Data Form (netCDF) format and based on the Climate and Forecast (CF) conventions and metadata. NetCDF is a self-describing, machine-independent data format that supports the creation, access, and sharing of array-oriented scientific data. The data format is "self-describing", which means that there is a header describing the layout of the rest of the file, in particular the data arrays, as well as arbitrary file metadata in the form of name/value attributes. The CF convention defines metadata that provide a definitive description of what the data in each variable represents, and of the spatial and temporal properties of the data. This enables users of data from different sources to decide which quantities are comparable, and facilitates building applications with extraction, re-gridding and display capabilities.

Software providing read/write access to netCDF files, encoding and decoding the necessary arrays and metadata are supplied by University Corporation for Atmospheric Research (UCAR) and others (<https://www.unidata.ucar.edu/software/netcdf>). A convenient viewer is Panoply (<https://www.giss.nasa.gov/tools/panoply>). Users preferring the Hierarchical Data Format (HDF) might use conversion tools (available at <https://www.hdfeos.org/software/tool.php#nco>).

The endianness (byte order) of product data is little-endian (the least-significant byte is stored first).

### 5.6.2 File-name convention

The SCE product files are named according to the following convention:

daily-multi-sce-<hemisphere>\_ease-50\_<year><month><day><hour><minutes>.nc

where

<hemisphere> is either 'nhl' (Northern Hemisphere land) or 'shl' (Southern Hemisphere land)

<year> is year of acquisition (Gregorian calendar)

<month> is month of acquisition (Gregorian calendar)

<day> is day of acquisition (Gregorian calendar)

<hour> is hour of acquisition (apparent solar time)

<minutes> is minutes of acquisition (apparent solar time)

Note that the time stamp <hour><minutes> is fixed to '1200' (meaning 12:00, noon, apparent solar time) is fixed and represent the local time of each grid cell for which the SCE value is an estimate for.

Example: 'daily-multi-sce-nhl\_ease-50\_200401011200.nc'  
is the daily (noon) SCE product for 1 January 2004 for the Northern Hemisphere.

### 5.6.3 Access

The products are stored at a file server with the Norwegian Meteorological Institute available through the CryoClim portal hosted by the Norwegian Computing Center. The portal web address is [www.cryoclim.net](http://www.cryoclim.net). For questions, please contact [cryoclim@nr.no](mailto:cryoclim@nr.no).

## 6 References

- Allen, R. C. Jr., Durkee, P. A., and Wash, C. H., 1990. Snow/cloud discrimination with multispectral satellite measurements. *Journal of Applied Meteorology and Climatology*, 29, 994–1004. [https://doi.org/10.1175/1520-0450\(1990\)029%3C0994:SDWMSM%3E2.0.CO;2](https://doi.org/10.1175/1520-0450(1990)029%3C0994:SDWMSM%3E2.0.CO;2)
- Armstrong, R. L., 2001. Historical Soviet Daily Snow Depth version 2 (HSDSD). National Snow and Ice Data Center, Boulder, CO, digital media. [Available online at <http://nsidc.org/data/g01092.html>.]
- Baum, L. E., Petrie, T., 1966. Statistical Inference for Probabilistic Functions of Finite State Markov Chains. *The Annals of Mathematical Statistics*, 37 (6), 1554–1563.
- Bicheron, P., Huc, M., Henry, C. and Bontemps, S., 2008. GLOBCOVER Products Description Manual. ESA Project GLOBCOVER, GLOBCOVER\_PDM\_I2.2, Issue 2, Revision 2.
- Bogaert, P., Waldner, F. and Defourny, P., 2016. An information-based criterion to measure pixel-level thematic uncertainty in land cover classifications. *Stoch Environ. Res. Risk Assess.*, Volume doi:10.1007/s00477-016-1310-y.
- Brown, K. M., Foody, G. M. and Atkinson, P. M., 2009. Estimating per-pixel thematic uncertainty in remote sensing classification. *Int. J. Remote Sensing*, 30(1), pp. 209-229.
- Brun, E., Vionnet, V., Boone, A., Decharme, B., Peings, Y., Valette, R., Karbou F. and Morin, S., 2013. Simulation of Northern Eurasian Local Snow Depth, Mass, and Density Using a Detailed Snowpack Model and Meteorological Reanalyses. *J. Hydrometeor*, 14, 203–219.
- Bulygina O. N., Korshunova N. N. and Razuvaev V. N., 2010. Climatic conditions over the territory of Russia. Online Information provided by the All-Russian Research Institute of Hydrometeorological Information of Federal Service for Hydrometeorology and Environmental Monitoring (available at <http://meteo.ru/english/climate/cl2009.php>) (Obninsk, Russia)
- Callaghan T.V., Johansson M., Prowse T.D., Olsen M.S. and Reiersen L.O., 2011. Arctic Cryosphere: Changes and Impacts”, *Ambio*, 40,3-5.
- Chang, A. T. C., Foster, J. L. and Hall, D. K., 1987. Nimbus-7 SMMR derived global snow cover parameters. *Annals of Glaciology*, 9, 39-44.
- Eastwood, S., et al. 2009. *OSI SAF Sea Ice Product Manual v3.6*. Oslo: Met.no.
- Fennig, K. 2016. Product User Manual Fundamental Climate Data Record of SMMR / SSMI / SSMIS Brightness Temperatures. EUMETSAT CM SAF document: [https://www.cmsaf.eu/SharedDocs/Literatur/document/2016/saf\\_cm\\_dwd\\_pum\\_fcdr\\_ssmi\\_1\\_1\\_pdf.html](https://www.cmsaf.eu/SharedDocs/Literatur/document/2016/saf_cm_dwd_pum_fcdr_ssmi_1_1_pdf.html)
- Fennig, K. 2017. Algorithm Theoretical Basis Document Fundamental Climate Data Record of SSM/I Brightness Temperatures Microwave Imager Radiance FCDR R3 CM-12002. EUMETSAT CM SAF document: [https://www.cmsaf.eu/SharedDocs/Literatur/document/2017/saf\\_cm\\_dwd\\_atbd\\_fcdr\\_ssmi\\_1\\_4\\_pdf.html](https://www.cmsaf.eu/SharedDocs/Literatur/document/2017/saf_cm_dwd_atbd_fcdr_ssmi_1_4_pdf.html)
- Foody, G. M., 2005. Local characterization of thematic classification accuracy spatially constrained confusion matrices. *Int. J. Remote Sensing*, Volume 26, pp. 1217-1228.

- Footy, G. M., Campbell, N. A., Trodd, N. A. and Wood, T. F., 1992. Derivation and application of probabilistic statistics of class membership from maximum-likelihood classification. *Photogramm. Engin. Remote Sensing*, Volume 58, pp. 1335-1341.
- Grody, N. C. and Bassist, A. N., 1996. Global identification of snow cover using SSM/I measurements. *IEEE Trans. Geosci. Remote Sensing* 34, no. 1: 237-249.
- Hiltbrunner, D. and Mätzler, C., 1997. Land surface temperature and snow discrimination using SSM/I data. Edited by S. Wunderle. *Proc. EARSeI Workshop "Remote Sensing of Land Ice and Snow"*. Freiburg im Breisgau, Germany: EARSeI, Paris: 87-94.
- Hollinger, J.P., Lo, R.C., Poe, G.A., Savage, R. and Peirce, J.L., 1987. Special Sensor Microwave/Imager User's Guide. Naval Research Laboratory, Washington D.C., USA.
- Janssen, L. L. F. and van der Wel, F. J. M., 1994. Accuracy assessment of satellite derived land-cover data: a review. *Photogramm. Engin. Remote Sensing*, Volume 60, pp. 419-426.
- Karlsson K.-G., Hanschmann, T., Stengel, M. and Meirink, J. F., 2016. Algorithm Theoretical Basis Document CM SAF Cloud, Albedo, Radiation data record, AVHRR-based, Edition 2 (CLARA-A2) Cloud Products (level-1 to level-3). EUMETSAT CM SAF document:  
[https://www.cmsaf.eu/SharedDocs/Literatur/document/2016/saf\\_cm\\_dwd\\_atbd\\_gac\\_cld\\_2\\_3\\_pdf.html](https://www.cmsaf.eu/SharedDocs/Literatur/document/2016/saf_cm_dwd_atbd_gac_cld_2_3_pdf.html)
- Karlsson K.-G., Sedlar, J., Devasthale, A., Stengel, M., Hanschmann, T., Meirink, J. F., Benas, N. and Zadelhoff, G.-J. van, 2017. Product User Manual CM SAF Cloud, Albedo, Radiation data record, AVHRR-based, Edition 2 (CLARA-A2) Cloud Products. EUMETSAT CM SAF document:  
[https://www.cmsaf.eu/SharedDocs/Literatur/document/2017/saf\\_cm\\_dwd\\_pum\\_gac\\_cld\\_2\\_3\\_pdf.html](https://www.cmsaf.eu/SharedDocs/Literatur/document/2017/saf_cm_dwd_pum_gac_cld_2_3_pdf.html)
- Killie, M.A., Godøy, Ø., Eastwood, S. and Laverne, T., 2011. ATBD for the EUMETSAT OSI SAF Regional Ice Edge Product, v1.1, SAF/OSI/CDOP/met.no/SCI/MA/135.
- Killie, M. A., Eastwood, S., Solberg, R., Rudjord, Ø. and Salberg, A.B., 2013. Snow sub-service development: Report on CryoClim WP 3 progress and results. Project deliverables no. D3.1-D3.10, CryoClim Phase 4, ESA/NSC PRODEX. Norwegian Computing Center and Norwegian Meteorological Institute.
- Killie, M. A., Eastwood, S. and Sørensen, A.M., 2018. Improvement and validation of the optical component used for global snow mapping in CryoClim, Sentinel4CryoClim Phase 2 Project Report, MET Report 12/2018.
- Krenke, A., 2004. Former Soviet Union hydrological snow surveys, 1966–1996. National Snow and Ice Data Center, Boulder, CO, digital media. [Available online at <http://nsidc.org/data/g01170.html>.]
- Künzi, K. F., Patil S. and Rott H., 1982. Snow-cover parameters retrieved from Nimbus-7 Scanning Multichannel Microwave Radiometer (SMMR) data. *IEEE Transactions on Geoscience and Remote Sensing*, 20, 452-467.
- Lemke, P. et al., 2007. *Observations: Changes in Snow, Ice and Frozen Ground*. In *Climate Change 2007: The Physical Science Basis*. Contribution of Working Group I to the 4th Assessment Report of IPCC. Cambridge Univ. Press, 337-383.

- Liu, G. W., Gopal, S. and Woodcock, C. E., 2004. Uncertainty and confidence in land cover classification using a hybrid classifier approach. *Photogramm. Engin. Remote Sensing*, Volume 70, pp. 963-971.
- Menne, M.J., Durre, I., Vose, R.S., Gleason, B.E. and Houston, T.G., 2012. An overview of the global historical climatology network-daily database. *J. Atmos. Oceanic Technol.* 29 (7), 897–910.
- Metsämäki, S., Salminen, M., Pulliainen, J., Luojus, K., Nagler, T., Bippus, G., Solberg, R., Salberg, A.-B., Trier, Ø. D. and Wiesmann, A. (2013). Algorithm Theoretical Basis Document – SE-algorithm. ESA GlobSnow project deliverable D09, ESRIN Contract 21703/08/I-EC.
- Njoku, E. G., Stacey, J. M. and Barath, F. T., 1980. The Seasat scanning multichannel microwave radiometer (SMMR): Instrument description and performance. *IEEE Journal of Oceanic Engineering*, 5, 100-115.
- NSIDC SMMR, 2018. Scanning Multi-channel Microwave Radiometer (SMMR). <https://nsidc.org/data/pm/smmr-instrument>
- NSIDC SSM/I, 2018. Special Sensor Microwave Imager (SSM/I). <https://nsidc.org/data/pm/ssmi-instrument>
- Ramsay, B.H., 1998. The interactive multisensor snow and ice mapping system. *Hydrological Processes*, 12, pp. 1537-1546.
- Robel, J., and Graumann, A. (ed.), 2014. NOAA KLM User's Guide. <https://www1.ncdc.noaa.gov/pub/data/satellite/publications/podguides/N-15%20thru%20N-19/pdf/0.0%20NOAA%20KLM%20Users%20Guide.pdf>
- Rudjord, Ø., Salberg, A.-B., Solberg, R., 2015. Global snow cover mapping using a multi-temporal multi-sensor approach. In *Proceedings of the 2015 8th International Workshop on the Analysis of Multitemporal Remote Sensing Images (Multi-Temp)*. DOI:10.1109/Multi-Temp.2015.7245775
- Salberg, A.-B., Solberg, R. (2022) ESA CCI+ Snow ECV, Option 2 - Fractional Snow Cover in CryoClim: Annex to End-to-End ECV Uncertainty Budget, version 2.0, July 2022.
- Serreze, M.C. et al., 2000. Observational evidence of recent change in the northern high-latitude. *Climatic Change*, 46 (1-2), 159-207
- Solberg, R, Huseby, R.B., Koren, H. and Malnes E., 2008. Time-series fusion of optical and SAR data for snow cover area mapping. *Proceedings of EARSeL LIS-SIG Workshop*, Berne, February 11-13 February, 2008.
- Solberg, R., Killie, M. Andreassen L. M. and König, M., 2014. CryoClim: A new system and service for climate monitoring of the cryosphere. *IOP Conf. Series: Earth and Environmental Science*, 17, 012008.
- Solberg R., Rudjord Ø., Salberg A.-B. and Killie M. A., 2015. Advancements and validation of a global snow product fusing optical and passive microwave radiometer data. *Proceedings for the 2015 EUMETSAT Meteorological Satellite Conference*, 21-25 September 2015, Toulouse, France.
- Solberg R., Rudjord Ø., Salberg, A.-B., Killie, M. A., Eastwood, S. and Breivik, L. A., 2018. Advancement of global snow mapping in CryoClim – Sentinel4CryoClim phase 2 report. NR Note SAMBA/44/18, Norwegian Computing Center.
- Solberg, R., Rudjord, Ø., Salberg, A.-B., Killie, M. A., Sørensen, A. M., Eastwood, S. (2022) ESA CCI+ Snow ECV, Option 2 - Fractional Snow Cover in CryoClim: Annex to Algorithm Theoretical Basis Document, version 2.0, July 2022.

- Viterbi, A. J., 1967. Error bounds for convolutional codes and an asymptotically optimum decoding algorithm. *IEEE Transactions on Information Theory*, 13 (2): 260–269. doi:10.1109/TIT.1967.1054010
- Wentz, F.J., (1988), User's Manual SSM/I Antenna Temperature Tapes. RSS Technical Report 032588, Remote Sensing Systems, Santa Rosa, CA, USA.

